

On the interaction of a vertical shear layer with a free surface

By DANA DABIRI

Department of Aeronautics and Astronautics, University of Washington,
206 Guggenheim, Box: 352400, Seattle, WA 98195, USA

(Received 3 June 2002 and in revised form 28 October 2002)

New experiments have been conducted using a combined free-surface gradient detector (FSGD) and digital particle image velocimetry (DPIV) technique to study the interaction between a vertical shear layer, created by a surface-piercing splitter plate, and a free surface. The emphasis of this study is on understanding aspects of the interaction between the free-surface deformation (FSD) and the near-surface turbulence through the correlations between the elevation and the vorticity fields, and the spectral behaviour of the near-surface pressure. The Reynolds number of the present study, based on visual thickness and the velocity average of the two streams, is 12 100. Mean results for the velocity and vorticity fields show that self-similarity is achieved. Instantaneous data sets show that at the free surface, vortex tubes within the main rollers connect normally with the free surface as is evidenced by strong vorticity as well as the strong deformations at the free surface. The instantaneous data sets also show that the streamwise vortices near the braid regions, while weaker than those seen in the main rollers, also reconnect with the free surface. Statistical analyses show that the FSD is strongly correlated with the near-surface vorticity field, as the correlation coefficients are quite high (~ 0.7 – 0.8). The pressure spectrum slope within the shear layer near the surface is found to be $-10/3$, compared with the analytically derived value of $-11/3$ (George *et al.* 1984) found for a shear layer in unbounded flow.

1. Introduction

Free-surface flows occur in many areas of interest, ranging from environmental and ocean sciences to hydrodynamics of ships. From an environmental point of view, the topic of free-surface flows is important in understanding the interaction between the atmosphere and the oceans. For example, it has been established that wave breaking, whether spilling or plunging, acts as a source of vorticity and turbulence generation, and thus bubble entrainment. In so doing, this process serves to enhance gas transfer from the atmosphere to the oceans, which is essential for supporting life underwater when considering O_2 and N_2 entrainment. Furthermore, since CO_2 is also considerably entrained, the oceans and their turbulent processes ultimately act as a sink for CO_2 from the atmosphere and therefore cannot be ignored (Melville 1996; Woolf & Thorpe 1991; Jähne & Haußecker 1998). From a more practical point of view, the interaction of the flow with a boat/ship hull and/or propellers produces both wave breaking and near-surface turbulence. For naval vessels, the results are ship wakes that extend for hundreds of kilometres, thereby making them detectable to remote sensing instruments. Understandably, this necessitates the need to study free surface turbulence in order to more fully understand and therefore control such flow patterns.

To date, much work has been done on near-surface flows. Numerical simulations and experiments have shown that as the free surface is approached from the bulk, the surface-normal velocity decreases while the lateral velocities increase (Brumley & Jirka 1987; Swain, Ramberg & Miner 1991; Sarpkaya & Neubert 1994). It has also been shown that there are two length scales near the free surface, initially discovered by Hunt & Graham (1978), which play an important role in vortex disconnection/reconnection. The first corresponds to an outer region, the source layer, where the surface normal fluctuations decrease, while the surface parallel components are amplified within one turbulence length scale beneath the free surface. The second corresponds to an inner viscous layer, where turbulent velocities decay to zero at the surface. Walker, Leighton & Garza-Rios (1996) also identified these two layers and found that the thickness of the source layer and viscous layer are the turbulence length scale and one-tenth the turbulence length scale respectively. By numerically studying a vortex ring obliquely approaching a free surface, Zhang, Shen & Yue (1999) found that these surface layers play a key role in the vortex/free surface reconnection via the surface boundary conditions they impose: the surface, or blockage layer, through vortex turning and stretching increase the vertical vorticity component, which then through viscous diffusion and further stretching, is transported through the viscous layer to the free surface. Shen *et al.* (1999) also point out that the surface layer is only present when horizontal vortex tubes approach the free surface. Making use of these results, Shen, Triantafyllou & Yue (2000) proposed a free-surface function model for large-eddy simulation (LES) modelling of free-surface turbulence. In an experimental study of a vortex ring obliquely approaching a free surface, Gharib *et al.* (1992) further suggest that the free-surface deformation plays a more active role in the reconnection process in that the associated accelerations generate secondary surface parallel vorticity (Lugt & Ohring 1992; Rood 1994), which interact with the part of the primary vortex ring nearest the free surface, initiating the disconnection/reconnection process. Other studies looking at the interaction between basic flows, such as jets, wakes, and shear layers, and a free surface have shown the development of a ‘surface current’, resulting from the anisotropy between the vertical and spanwise kinetic energies (Walker & Johnston 1991; Anthony & Willmarth 1992; Walker *et al.* 1996; Logory, Hirska & Anthony 1996; Maheo 1999). Surface currents have also been seen in solid wall/free surface junctures (Grega *et al.* 1995; Longo, Huang & Stern 1998).

While much work has been done to aid our understanding of near-surface turbulence, little has been done to study how the free-surface deformations (FSDs) are related to the near-surface turbulence. Shadowgraph pictures have shown that the free surface deforms as a vortex tube, whether perpendicular or parallel to the free surface, approaches the free surface (Bernal & Kwon 1989; Sarpkaya & Suthon 1991; Gharib & Weigand 1996; Willert & Gharib 1997). Dommermuth, Novikov & Mui (1994) show that for low Froude number flows, the equations of motion can be expressed as

$$\frac{\partial U_i^r}{\partial \tilde{t}} + U_j^r \frac{\partial U_i^r}{\partial x_j} = -\frac{\partial P^r}{\partial \tilde{x}_i} + \frac{1}{Re} \frac{\partial^2 U_i^r}{\partial x_j^2} + \alpha f(U_i^r), \quad (1.1)$$

$$\frac{\partial U_i^r}{\partial \tilde{x}_i} = 0; \quad \frac{\partial^2 P^r}{\partial x_j^2} = -\frac{\partial U_j^r}{\partial \tilde{x}_i} \frac{\partial U_i^r}{\partial \tilde{x}_j} \quad \text{for } \tilde{z} \leq 0; \quad (1.2)$$

$$\frac{1}{Fr^2} \eta^r = -P_a + P^r \quad \text{for } \tilde{z} = 0 \quad (1.3)$$

where the superscript r refers to components that contribute to the free-surface roughness, η is the free-surface elevation, P is the pressure normalized by the density, U is the velocity, the subscript a refers to atmospheric conditions, α is a source coefficient, f is a linear operator, and \tilde{x}_j and \tilde{t}_j correspond to long length and time scales such that $\partial\tilde{x}_j = Fr^2\partial x_j$ and $\partial\tilde{t}_j = Fr^2\partial t_j$. The last of these equations shows that with the neglect of the atmospheric pressure, ‘the surface elevation is hydrostatically balanced by the vorticity-induced pressure’, implying that there should be a strong correlation between vorticity and the FSD. However, by comparing initial and final states of the vortical pressure and surface-normal vorticity fields, Dommermuth (1994) concludes that they are in fact poorly correlated. Zhang *et al.* (1999) also suggest that the surface vertical vorticity and free-surface elevation are not necessarily well-correlated, since contour shapes and maximum positions do not necessarily correspond. Tsai (1998), using simulations and statistical averaging, shows that the correlation between the vertical vorticity component and the FSD is low ($\sim 50\text{--}60\%$). On the other hand, simultaneous and instantaneous shadowgraph and digital particle image velocimetry (DPIV) measurements, though qualitative, show that individual vortices correlate well with surface dimples shown (Weigand & Gharib 1995), suggesting that these correlations may be statistically higher than simulations have shown.

On a different note, equation (1.3) allows measurement of near-surface pressures by direct measurements of the free-surface elevations, and thereby the obtaining of pressure spectra. Monin & Yaglom (1975) have shown that for grid-generated turbulence, the pressure spectra shows a $-7/3$ slope in the inertial subrange. Beuther, George & Arndt (1977*a, b*) and George, Beuther & Arndt (1984) showed that for the case of homogeneous constant-mean-shear flows, the spectrum is composed of three terms: a turbulence–turbulence interaction with a $-7/3$ slope as previously found by Monin & Yaglom (1975), a dominant second-moment turbulence–mean-shear interaction term with a $-11/3$ slope, and a third-moment turbulence–mean-shear interaction term with a -3 slope, which might be significant at low wavenumbers in high Reynolds number flows. By inferring the pressure spectra from the free-surface elevation measurements, the nature of the inertial-subrange distribution for this flow can be established and compared with previous results.

In order to further our understanding of near-surface flow interaction with a free surface, this work is aimed at answering the following questions: As vortical pressure is directly responsible for the FSD, can it experimentally be verified that vorticity and FSD are in fact highly correlated? Furthermore, what is the spectrum of the free-surface pressure for this flow? To answer these questions, the present work investigates the interaction of a vertical shear layer, generated by a surface-piercing splitter plate, with a free surface. The experimental setup is first explained in §2 by describing the DPIV and free-surface gradient detector (FSGD) setup used to simultaneously acquire kinematic and FSD data. The flow and surface deformation structures are then described by examining instantaneous data in §3. Section 4 characterizes the flow behaviour through statistical measurements of the mean quantities (§4.1) and correlation quantities (§4.2), and by examination of the pressure spectra (§4.3).

2. Experimental setup

The experimental work was performed in a free-surface shear layer facility at the Graduate Aeronautical laboratories at the California Institute of Technology (see figure 1). The test section of the tunnel is 2 m long, 1 m wide, and 0.75 m high. As

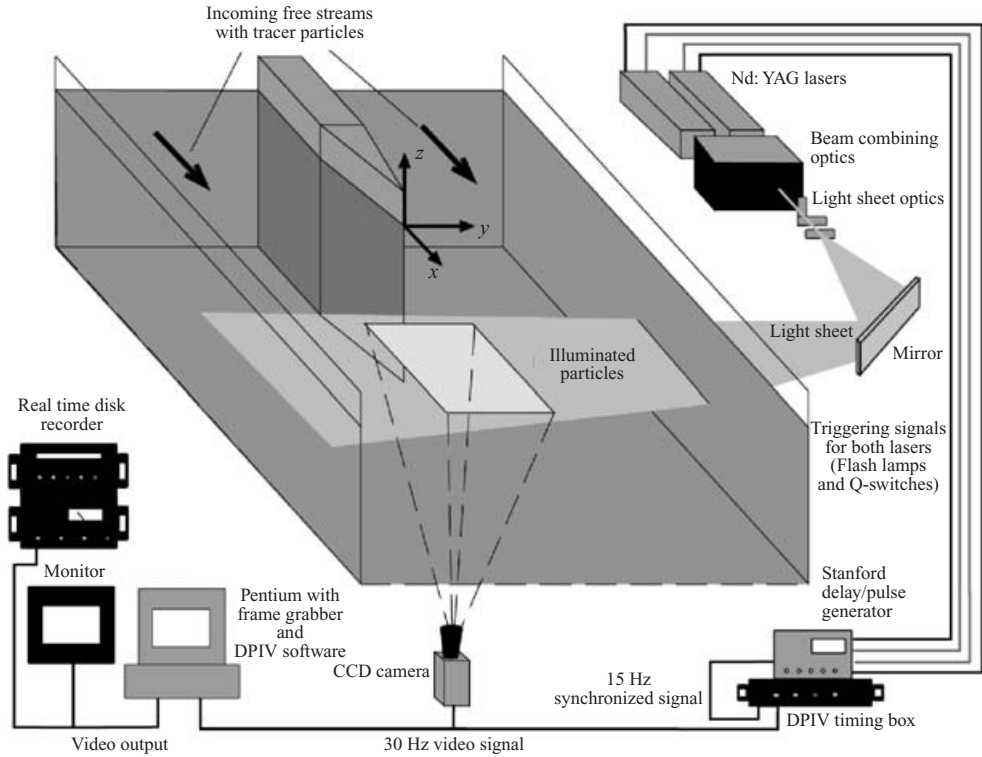


FIGURE 1. Free shear tunnel facility with DPIV experimental setup.

shown, x corresponds to the streamwise direction, y corresponds to the transverse direction, and z corresponds to the vertical direction. At rest, the water level is 56 cm high. A combined FSGD and DPIV system is used to map both the FSD and the near-surface kinematic fields. For the DPIV measurements, a horizontal laser light sheet is generated using a Nd:YAG laser 1 mm below the free surface, with respect to the free-stream fluid that is not deforming, allowing acquisition of the streamwise and transverse (u, v) velocity components, as well as the calculation of the vertical vorticity component. 14.0 micrometre silver-coated hollow glass sphere particles are used to seed the flow. The DPIV camera images a 22 cm by 22 cm area onto a 1008×1018 pixel array. These images are processed using 32×32 pixel interrogation window sizes ($6.9 \text{ mm} \times 6.9 \text{ mm}$) with a 50% overlap (3.45 mm step size). The smallest vortices seen near the braid and the roller regions (to be discussed in the following section) are 15 mm and 20 mm, respectively, thereby being adequately resolved with the DPIV method.

The FSGD measurement technique is based on the simultaneous two-component slope colour-encoding scheme developed by Zhang & Cox (1994). The experimental setup for the FSGD is shown in figure 2. This setup is mounted on the free-surface water tunnel facility, directly over the area of interest. Since the Froude number is low and the FSDs are small, a reflective scheme is used (Dabiri, Zhang & Gharib 1994, 1997). The maximum elevation measured by the FSGD is 1.4 mm. Most recently, a continuous colour palette (Jähne 1997; Balschbach, Klinke & Jähne 1998) is used rather than a discrete colour palette as it allows more accurate measurements (Dabiri & Gharib 2001).

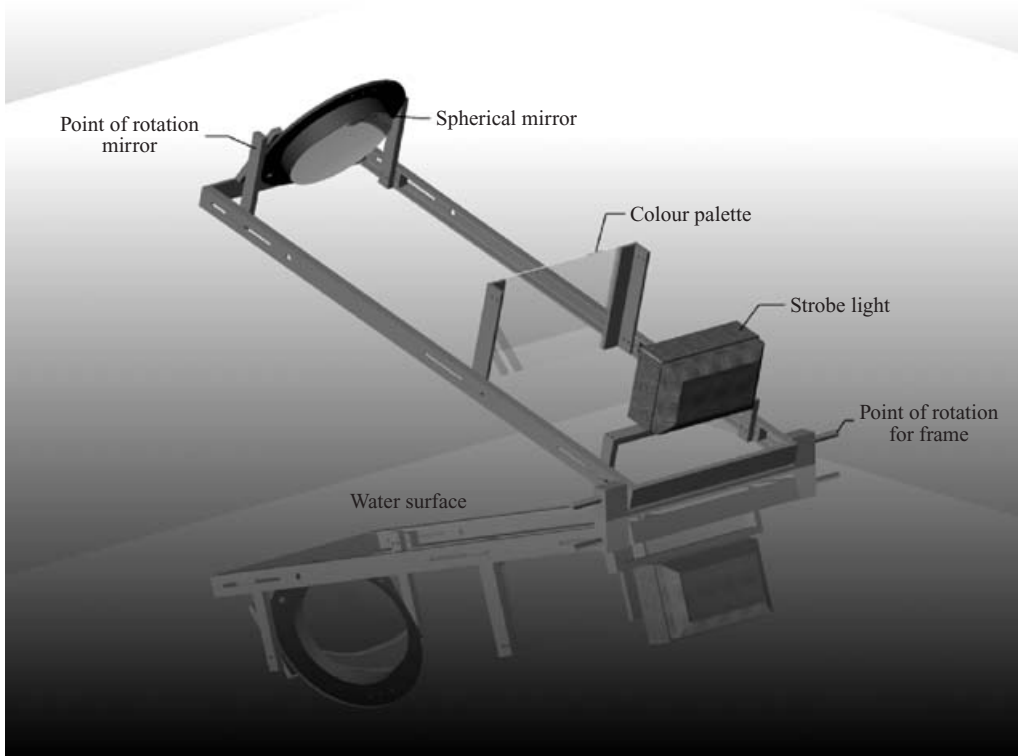


FIGURE 2. Free-surface gradient detector setup.

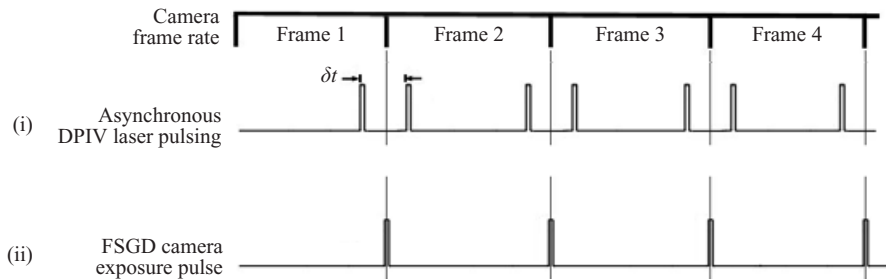


FIGURE 3. FSGD and DPIV timing synchronization diagram.

Since both the FSGD and DPIV systems must acquire data simultaneously, both systems are synchronized by placing the FSGD exposure pulse between the two DPIV exposure pulses (figure 3). The uncertainty in the velocity is less than 1% of the high-speed-stream velocity, and the maximum uncertainty of the FSGD is less than 6% of the maximum detectable gradient. Further details of this method can be found in Dabiri & Gharib (2001).

The tunnel is run with the high-speed side at $U_1 = 22.5 \text{ cm s}^{-1}$, and the low-speed side at $U_2 = 10.5 \text{ cm s}^{-1}$. The displayed area is $22 \times 18 \text{ cm}^2$, and the centre of this area is located 35.5 cm away from the end of the splitter plate. The flow in the tunnel moves all the surface contaminants to the end, where small suction devices remove them. The vorticity thickness, δ_ω , defined as the ratio of ΔU , the high- and low-speed free-stream velocity difference, to $(\partial U / \partial y)|_{max}$, the maximum average velocity gradient,

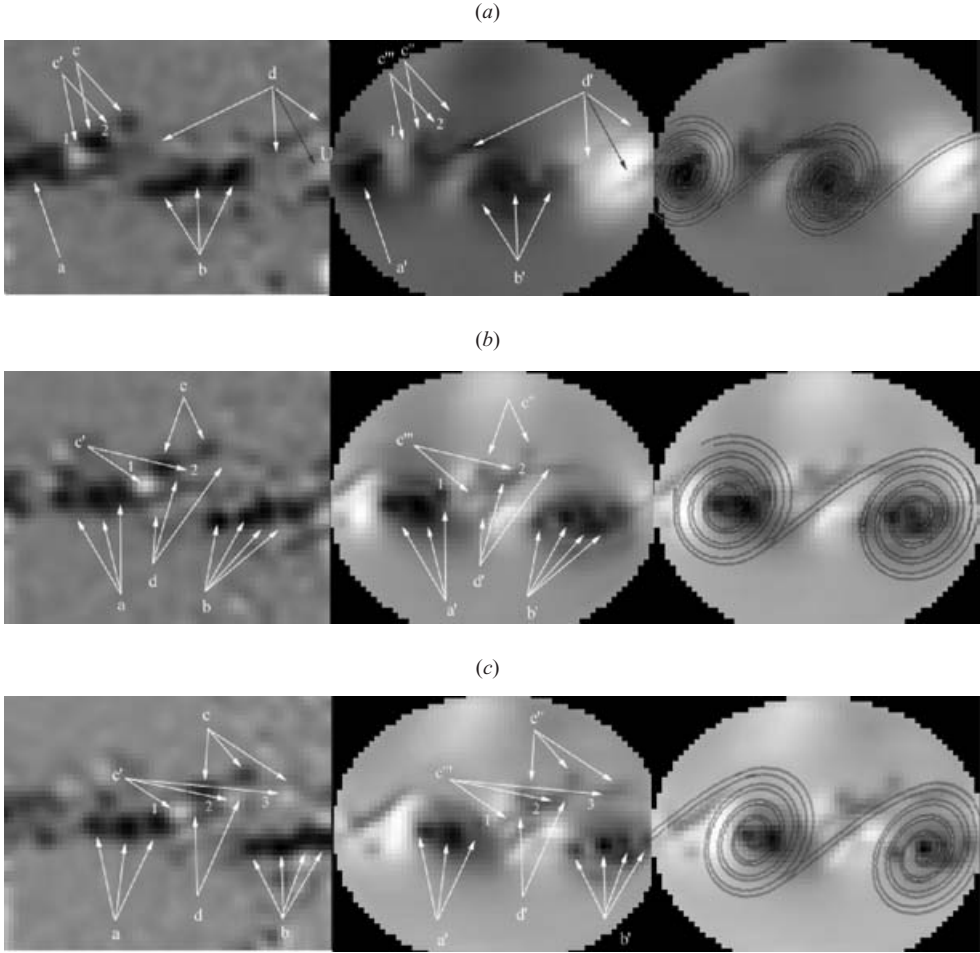


FIGURE 4. Instantaneous vorticity (left) and FSD (centre and right) plot at (a) $t = 0$, (b) $t = 0.267$ s; and (c) $t = 0.4$ s. The flow is from left to right; the high-speed side is on the top, and low speed side is on the bottom. Each of the images shows an area 22 cm wide by 18 cm high. The velocity ratio, U_2/U_1 , is 0.467, and the vorticity thickness is 4.5 cm. The FSD on the right includes graphically drawn spirals to show the location of the main rollers in relation to the FSD.

at mid-image, is 4.5 cm. The visual velocity thickness, $\delta_{0.99}$, defined as the spanwise thickness of the shear layer between 99% of the high-speed velocity, and 101% of the low-speed velocity, at mid-image is 7.35 cm. The local Reynolds number, based on the average velocity of the two streams and the vorticity thickness of the shear layer at the surface at mid-image, δ_ω , is therefore 7400, while the local Reynolds number, based on the average velocity of the two streams and the visual velocity thickness, is 12 100. The Froude number, based on the velocity of the high-speed side and the depth of the water channel is 0.07. A total of 2700 sequential data sets were averaged in order to obtain the statistical quantities discussed below.

3. Quantitative flow visualization of surface structures

The basic structure and development of the present shear layer is explained in a short sequence of instantaneous images (figures 4a–4c). The instantaneous vorticity

field is shown on the left and the FSD field is shown in the centre and on the right. As these instantaneous flow fields might not show the location of the main rollers as well as a video would, the FSD image is repeated in the right of figures 4(a)–4(c), with graphically overlaid spirals showing the main roller locations. The flow within each image of the figures is from left to right; the high-speed side is on the top and the low-speed side is on the bottom, showing an area 22 cm wide by 18 cm high. The darker regions on the vorticity plots correspond to more-negative vorticity values, while the brighter regions correspond to more-positive vorticity values. Likewise, for the FSD plots, the darker regions correspond to deeper free-surface depressions, while the brighter regions correspond to higher free-surface elevations.

On general observation of this sequence, it is seen that the main rollers contain several small vortices that have reconnected to the free surface. For this particular sequence, these vortices are located linearly within each of the rollers. This is not consistently the case as most often these vortices are found to be randomly distributed within the main roller. This sequence has been chosen for presentation since the distribution of the small vortices allows a clear identification and explanation of the flow features presented below.

Figure 4(a), at $t = 0$, shows that the main turbulent rollers of the shear layer contain several smaller vortices, labelled a and b, at the free surface. The FSD shows that there are corresponding depressions, as indicated by the dark region labelled a' and the dark dots labelled b', due to vortices a and b, indicating that these vortices have reconnected with the free surface. The FSD also shows that around the group of vortices denoted by b is a larger though less shallow depression, as indicated by its brighter shade of grey. This corresponds to the larger depression that is due to the main roller as shown in the rightmost image of figure 4(a). The interaction of the braid region with the free surface is labelled d'. Interestingly, the corresponding vorticity labelled d does not have appreciable levels compared to those seen within the vortices of the main roller. Further examination of these images shows the existence of strong negative vorticity outside the rollers, labelled c, which is accompanied by positive vortices, labelled c'. Their corresponding FSDs are labelled c'' and c'''. Examination of the FSD plots shows that these vortices, while generating very shallow deformations at the free surface, are attached to the braid region, d', and might therefore be streamwise vortex structures that ride on the braid region (Bernal & Roshko 1986). Due to their interaction with the free surface, these streamwise vortices, c and c'', connect vertically to the free surface in satisfaction of the free-surface slip condition. A description of this process will be given at the end of this section. The negative component of the streamwise vortices, c, upon connection with the free surface, produces distinct dimples on the free surface, c''. However, the positive component of the streamwise vortices, c', does not seem to produce such distinct results: c'1, the stronger of the two positive vortices, produces within its local surroundings an elevated region, c''', while c'2, the weaker of the two positive vortices, has not deformed the free surface at all.

Figure 4(b) shows the evolution of the flow at $t = 0.267$ s. The vortices within the main rollers, see a and b and the rightmost image, are seen to still be distinct. In fact, not only have the vortices within the main roller, labelled a and b, become more pronounced, but their deformations on the free surface, labelled in the central image by a' and b', have become much more pronounced, indicating a much stronger vertical connection with the free surface. Also, as seen in the central image of figure 4(a), the central image of figure 4(b) also shows a larger and shallower depression surrounding the group of the a' and b' vortex dimples, indicating that the deformation

is due to the main rollers of the shear layer, as shown in the rightmost image of figure 4(b). The interaction of the braid region with the free surface is labelled d' . Similarly to figure 4(a), the corresponding vorticity, d , does not have vorticity levels as strong as those seen by the vertical connections of the vortex tubes shown by a , a' and b , b' . The streamwise vortices, c , have a stronger connection with the free surface, c'' , as their connection with the braid region becomes stronger. The positive vorticity component, c' , has also connected more strongly with the free surface, as is evident by the free-surface dimple c''' . As was seen in figure 4(a), this dimple is also seen to be surrounded by an elevated region. This is due to the fact that $c'1$, located within a region of negative vorticity, rotates in an opposite direction, thereby creating around its perimeter a circumference of fluid with higher pressure, and therefore higher elevation.

Figure 4(c), at $t = 0.4$ s, shows the last step of the evolution in this sequence. Of the three main vortices that are seen in the main roller, labelled a , the right most vortex is seen to have begun to detach from the free surface as its depression upon the free surface, a' , is lessened. The vortices b have maintained their connections with the free surface as shown by b' in the central image. The vorticity and FSD associated with the braid region, d and d' , continue to show weak correlations, as no appreciable levels of vorticity can be found, and therefore can be shown to be responsible for the braid region deformation indicated by d' . This trend therefore suggests that the FSD correlates better with the vertically connecting vortices than with the vorticity associated with the braid region. The streamwise vortex structures, c , c' , c'' , c''' , continue to remain connected with the free surface, as discussed in figure 4(b). In figure 4(c) a new streamwise vortex is seen to connect to the free surface, and is labelled with arrow 3 of c' and c''' ; $c'1$ still maintains strong positive vorticity, and deformation, $c'''1$, as previously described in figure 4(b), while the weaker positive vortices, $c'2$, do not show noticeable a deformation, as seen by $c'''2$.

Using figures 5(a) and 5(b), a process for the development of vortices in c , c' , c'' , and c''' in figures 4(a)–4(c) is proposed. Any small perturbation within the shear layer will cause kinks within the axis of the streamwise vortices, as shown in figure 5(a). For the near-surface streamwise vortices, as these kinks approach the free surface they reattach to the free surface as explained by Gharib & Weigand (1996), and Willert & Gharib (1997), resulting in vortex pairs attached to the braid region, as shown in figure 5(b). The process of reconnection of the streamwise vortices as described here is believed to be responsible for the vortex pairs c and c' , resulting in the deformations c'' and c''' .

4. Results

In the following subsections, statistical results are presented in order to characterize the dynamics of the near-surface turbulence. Section 4.1 discusses mean quantities, §4.2 discusses correlation quantities, and §4.3 discusses the pressure spectra. The data in these sections have been rescaled so that the shear layer dividing streamline, as defined by

$$\int_{y_0}^{\infty} \rho u (U_1 - u) dy = \int_{-\infty}^{y_0} \rho u (u - U_2) dy,$$

where U_1 is the high-speed velocity, U_2 is the low-speed velocity, ρ is the fluid density, and y_0 is the y -coordinate of the dividing streamline, is located at the origin on the y -axis (spanwise direction). The low-speed side is on the negative y -axis, while the high-speed side is on the positive y -axis. The y -axis has also been normalized by

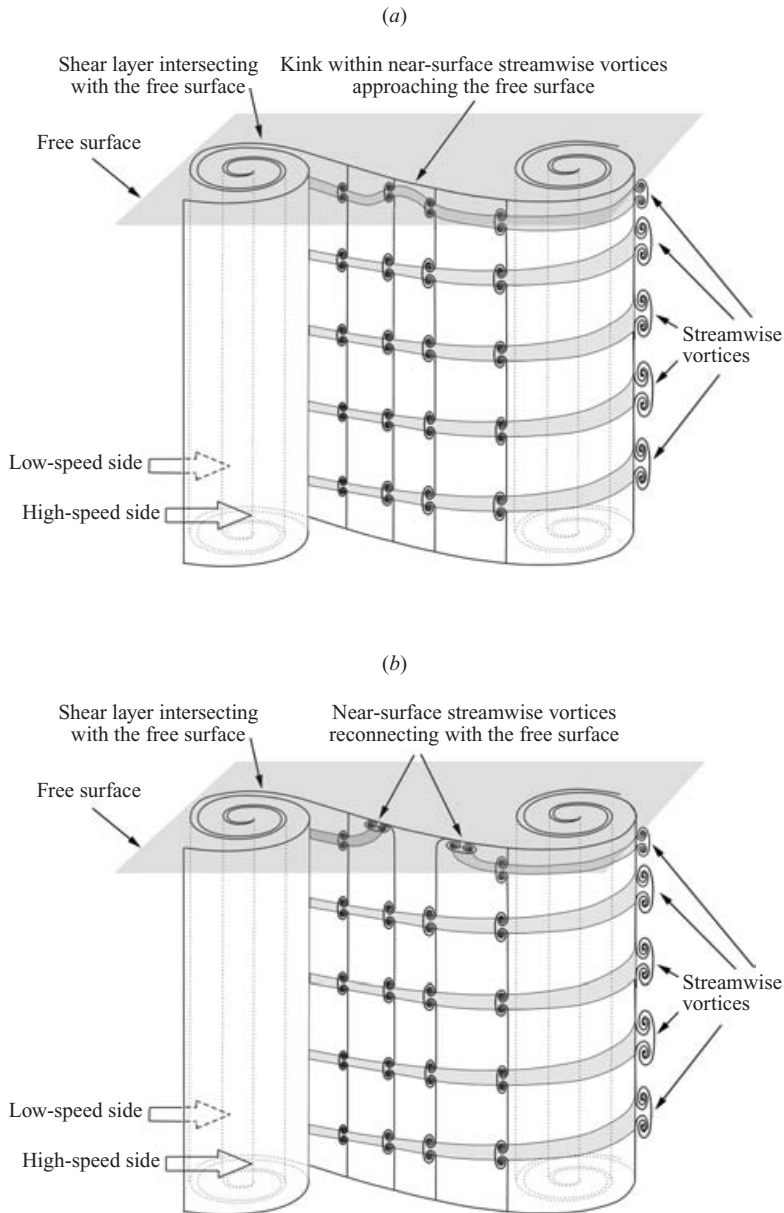


FIGURE 5. Schematic drawing showing the streamwise vortices within the braid region of the shear layer. (a) The beginning of the process of reconnection of the near-surface streamwise vorticity with the free-surface as its kink approaches the free surface. (b) The completion of the reconnection process of the near-surface vorticity with the free surface, resulting in the appearance of two vortex pairs at the free surface.

the similarity variable, λ , where $\lambda = y/\delta_\omega$, and δ_ω is the free-surface vorticity thickness. The domain is in the range $\lambda \in [-3, 3]$ in the spanwise direction, and $x/\theta \in [72, 126]$ in the streamwise direction, where θ is the momentum thickness of the boundary layer on the splitter plate. Six spanwise profiles are extracted from the domain at $x/\theta = 72.7, 84.5, 96.3, 108.1, 115.9, 125.8$ in order to explain the different features and downstream development of the flow for the various cases described below.

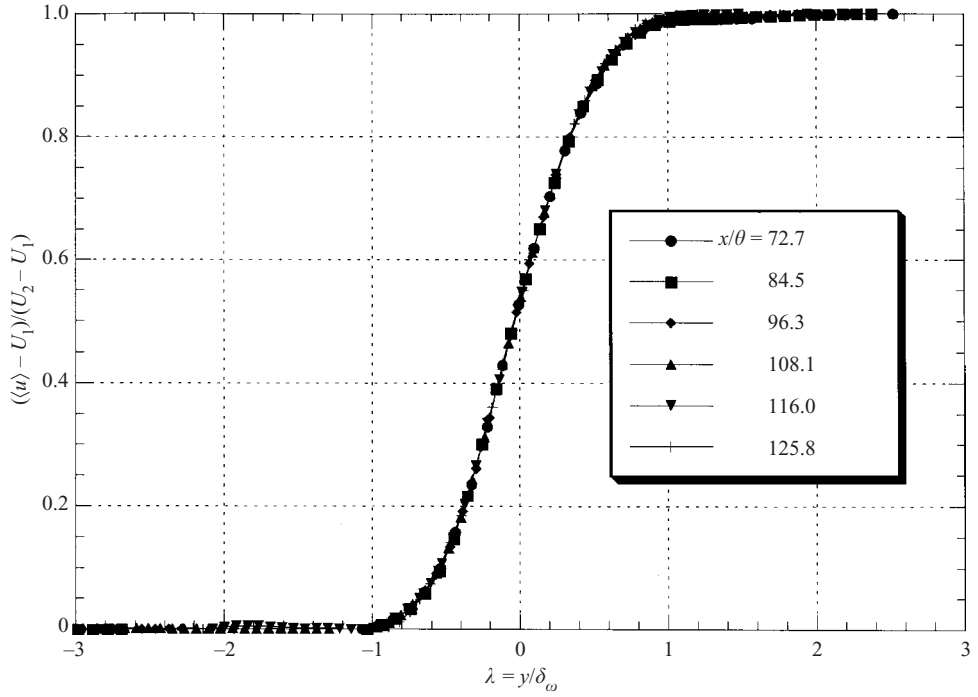


FIGURE 6. Mean normalized streamwise velocity profiles at various downstream locations.

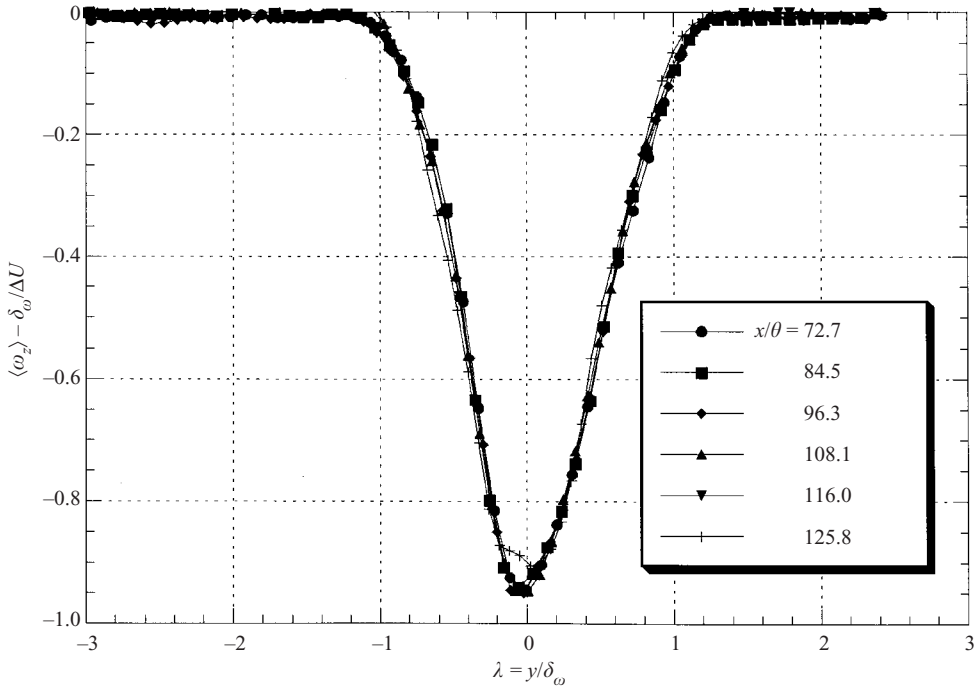


FIGURE 7. Mean normalized vertical vorticity profiles at various downstream locations.

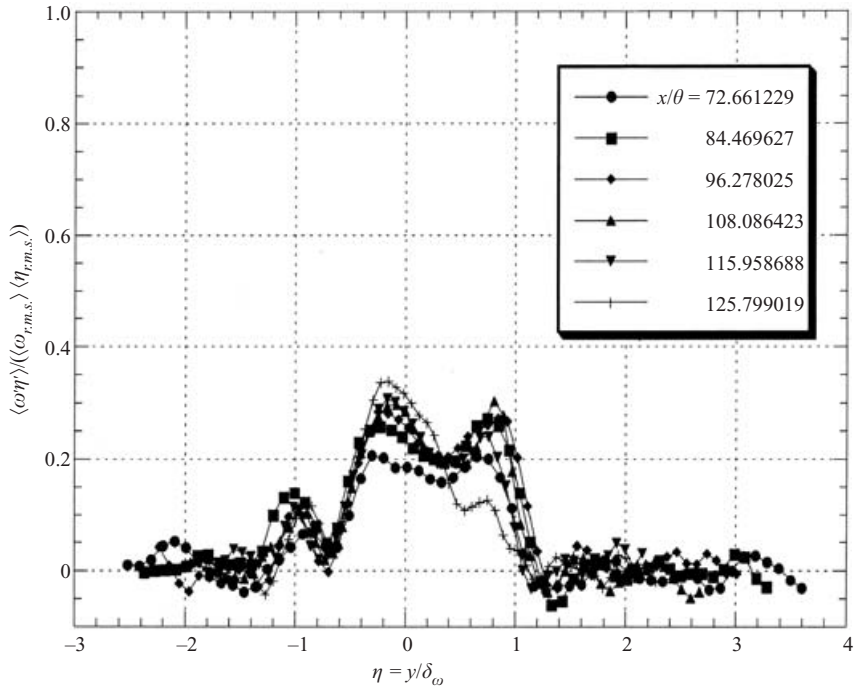


FIGURE 8. Mean vertical vorticity–elevation correlation coefficient profiles at various downstream locations.

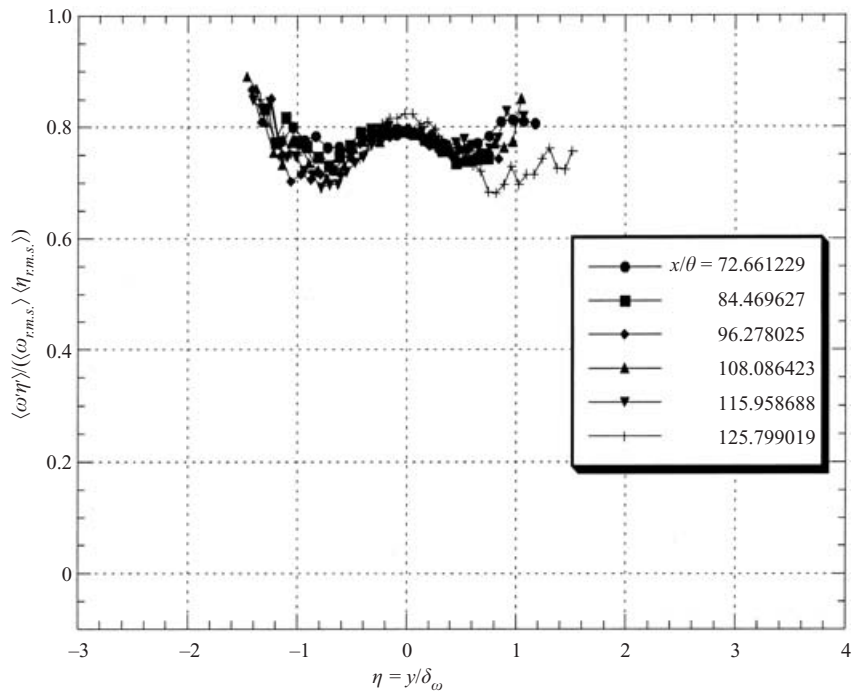


FIGURE 9. Mean vertical conditional vorticity–elevation correlation coefficient profiles at various downstream locations. Only vorticity within the range $[-15, -1.0]$, and negative elevation values are correlated.

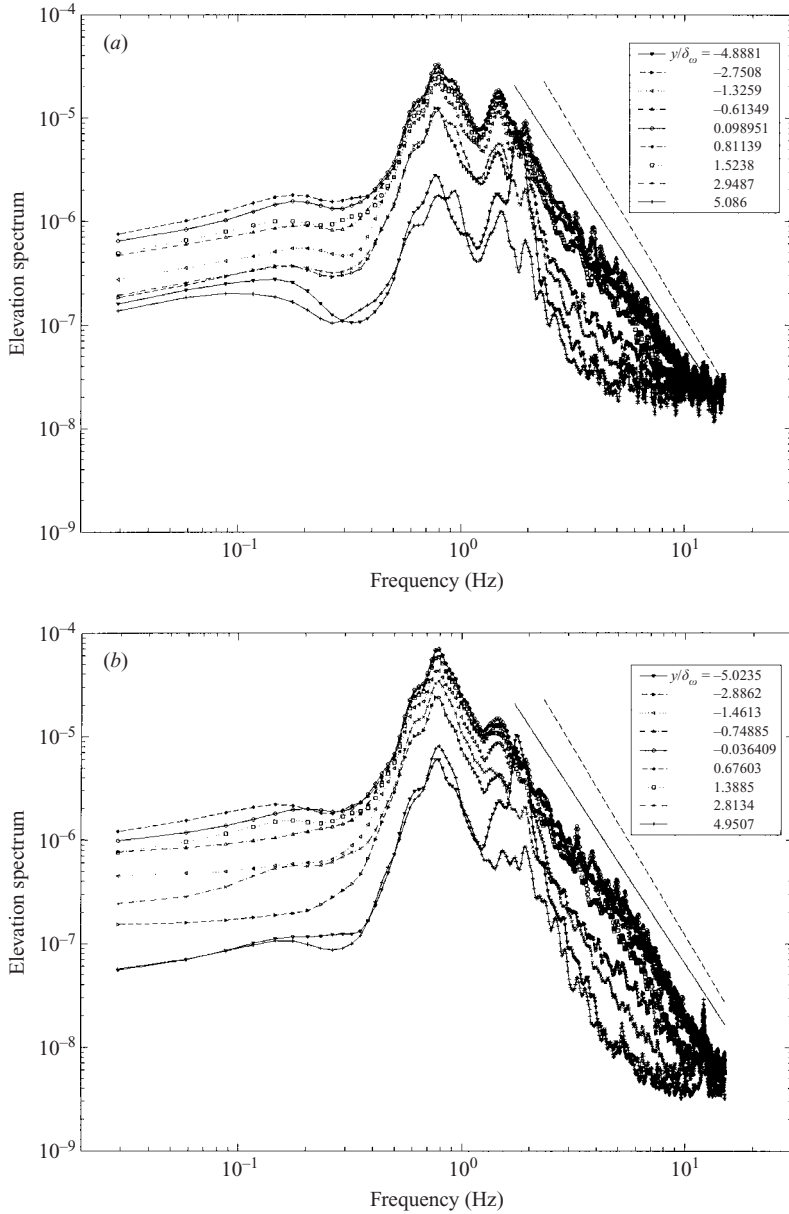


FIGURE 10(a,b). For caption see facing page.

4.1. Discussion of mean results

Figure 6 shows the average normalized streamwise velocity profile at different downstream locations. The normalized profiles show that all downstream locations within the imaged area have nicely collapsed onto a single curve, demonstrating that the flow is self-preserving in the mean. The normalized velocity profile varies from 0 to 1 within the range $-1 \leq \lambda \leq 1$, thus defining the domain of the shear layer in the mean. Figure 7 shows the average vorticity at various downstream locations, normalized by $\delta_\omega/\Delta U$ where ΔU is the velocity difference of the two free streams. These results have also collapsed onto a single curve, showing that a self-preserving

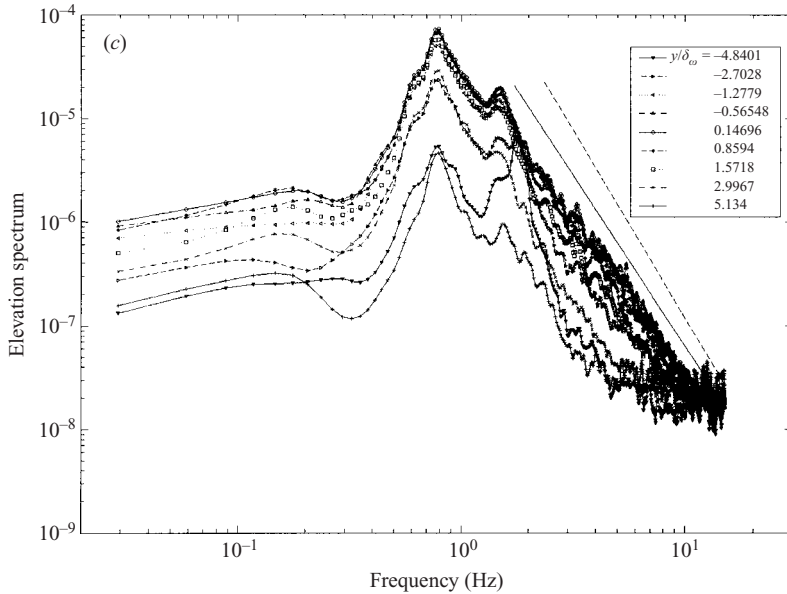


FIGURE 10. Spanwise pressure spectra for various spanwise locations, y/δ_ω at (a) $x/\theta = 66.3$, (b) $x/\theta = 96.8$ and (c) $x/\theta = 111.8$.

state in the mean has been achieved. In both these cases, it is seen that all non-zero values and therefore flow phenomena occurring in the mean are within $-1 \leq \lambda \leq 1$, with the half-height width equal to δ_ω . Further examination shows that this curve is slightly skewed to the low-speed side such that its peak value is located at $\lambda = -0.05$. This slight skewness is believed to be a characteristic of the flow facility.

4.2. Discussion of correlation results

The surface-normal vorticity correlation coefficients are shown in figure 8. For $-1 \leq \lambda \leq 1$, the correlation coefficients range within $[0, 0.2]$, indicating a weak correlation between the surface-normal vorticity and the free-surface elevation. These results would therefore appear to support the findings of Dommermuth (1994) and Zhang *et al.* (1999), who also concluded that surface-normal vorticity and free surface elevation are poorly correlated.

On reflection, however, aside from free-surface deformations due to vortex/free-surface interactions, the free surface can also rise or fall due to other turbulent features of the shear layer. Furthermore, as a vortex creates a low-pressure centre, a vortex connecting with the free surface will lower the elevation from its rest position, thereby creating a 'negative' elevation value. Moreover, due to the setup of the shear layer, the mean surface-normal vorticity will be negative (see figure 7), thereby creating negative-valued vortices. Therefore, given these considerations, surface-normal vorticity and free-surface elevations should be conditionally correlated, such that only simultaneously existing negative-valued free-surface elevations and negative-valued surface-normal vorticity are used in the correlation. This will then isolate the surface-normal vorticity and the negative elevations from all other aspects of the flow so that an accurate test of this correlation can be made. Figure 9 shows this correlation where negative elevation values were correlated with negative vorticity within the range $[-15.0 \text{ s}^{-1}, -1.0 \text{ s}^{-1}]$. This plot shows that the correlation coefficients for $-1 \leq \lambda \leq 1$ dramatically increase to $[0.7, 0.8]$, indicating that in fact the

surface-normal vorticity and the free-surface elevation are strongly correlated. Outside this range, there are no correlation coefficients as there were no contributing data points.

4.3. Spectral behaviour of the pressure fluctuations

In this section, the pressure spectra (figures 10(a)–10(c)) are shown at several spanwise locations for three streamwise locations: $x/\theta = 66.3, 96.85, 111.8$. The purpose of these images is to identify spectral variations as a function of streamwise location. For these plots, within the inertial range, the spectra show a logarithmic distribution for $-1.5 \leq \lambda \leq 1.5$. Outside this range, the spectra drop in amplitude within the inertial domain, except for the peak seen at ~ 0.1 Hz which corresponds to the sloshing frequency of the free-surface water tunnel facility. As the behaviours of these three plots are very similar, the pressure spectral behaviour does not change through the observed downstream distance, indicating possible self-similarity in the pressure. Within the spanwise range $-1.5 \leq \lambda \leq 1.5$, the slope is closer to $-10/3$ rather than $-11/3$, as shown by the black and blue lines, respectively, in figure 10. As it is impossible to separate the effects of the second-moment turbulence–mean shear interaction from the third-moment turbulence–mean-shear interaction and the turbulence–turbulence interaction as described by George *et al.* (1984), the present measurement is the result of all three terms combined, and therefore the theoretical slope due to the second-moment turbulence–mean shear interaction cannot be isolated. This argument, however, assumes that the pressure variations due to the influence of the free surface are small. As pressure measurements are not available across the shear layer within the fluid bulk, the influence of the free surface on an otherwise undisturbed shear layer remains an open question, and therefore a topic for further study.

5. Summary and conclusions

The study the interaction of a vertical shear layer with a free surface has been made possible using a novel measurement system integrating and synchronizing the FSGD and the DPIV techniques. The local Reynolds numbers based on the vorticity thickness and visual velocity thickness are 7400 and 12 100, respectively. The Froude number based on the velocity of the high-speed side and the tunnel's water depth is 0.07. Sequences of instantaneous plots of the vorticity and the FSD show that for the measured area, the main rollers are composed of several smaller clusters of persistent vortices connected to the free surface, which are not apparent in fully submerged shear flows, as seen by other shear layer flow visualizations such as the shadowgraphs of Brown & Roshko (1974). Each of the vortices within these clusters contributes to a general deformation about each of the main rollers that is due to their respective integrated pressure field. Furthermore, vortices near the braid region are also seen attached to the free surface. It is postulated that these vortices are the streamwise vortices, which due to being near the surface, turn and reconnect with the free surface.

Normalized mean spanwise velocity and vorticity profiles at several different downstream positions show that these profiles collapse onto a single curve, signifying that the flow is self-preserving in the mean. It is also shown that negative-valued vorticity must be conditionally correlated with simultaneously occurring free-surface depressions in order to accurately measure the correlation coefficient. Using this approach, it is found that the correlation coefficient is within the range [0.7, 0.8], and is therefore quite high, contrary to previously published results.

While the kinematic properties were mostly confined to $-1 \leq \lambda \leq 1$, the pressure fluctuation spectra show a full inertial distribution for $-1.5 \leq \lambda \leq 1.5$, as pressure effects are felt more globally than locally. Unlike previous findings, the present work shows that the free-surface deformation is strongly correlated with the surface-normal vorticity. The slope of the spectra in this inertial range was also found to be $-10/3$, compared to the analytically derived value of $-11/3$ of George *et al.* for unbounded shear layers.

In the future, the FSGD with 3D-DPIV (Pereira *et al.* 2000) will be integrated in order to obtain all three velocity components, as well as the full deformation matrix. This will further allow quantitatively testing of our hypothesis that the near-surface streamwise braided vortices of the shear layer reattach normally to the shear layer, as is believed to have been seen in the present work. Furthermore, this will also allow identification of vortical tubes both parallel and perpendicular to the free surface, and determination of the role of all components of vorticity in the free surface deformation. Lastly, the calculation of the near-surface pressure from the free-surface elevation measurements will also provide an opportunity to measure the pressure-strain terms in the turbulent kinetic energy equation, and to determine its role in the dynamic evolution of the turbulence near the free surface.

The author would like to thank Patrice Maheo for allowing the use of figure 1 from his thesis, which was used to describe the same facility used for both our projects. The author also acknowledges the comments of the reviewers whose insights have added to this paper. The author gratefully acknowledges the support of the Office of Naval Research under the research grant number N00014-97-1-0303.

REFERENCES

- ANTHONY, D. G. & WILLMARTH, W. W. 1992 Turbulence measurements in a round jet beneath a free-surface. *J. Fluid Mech.* **243**, 699–720
- BALSCHBACH, G., KLINKE, J. & JÄHNE, B. 1998 Multichannel shape from shading techniques for moving specular surfaces. *Computer Vision (ECCV '98), Proc.* Vol. II, (ed. H. Burkhardt & B. Neumann). Lecture Notes in Computer Science, vol. 1407, pp. 170–184. Springer.
- BERNAL, L. P. & KWON, J. T. 1989 Vortex ring dynamics at a free surface. *Phys. Fluids A* **1**, 449–451.
- BERNAL, L. P. & ROSHKO, A. 1986 Streamwise vortex structure in plane mixing layers. *J. Fluid Mech.* **170**, 499–525.
- BEUTHER, P. D., GEORGE, W. K. & ARNDT, R. E. A. 1977a Modeling of pressure spectra in a turbulent shear flow. *J. Acoust. Soc. Am.* **61**, 524, Suppl. 1.
- BEUTHER, P. D., GEORGE, W. K. & ARNDT, R. E. A. 1977b Pressure spectra in a turbulent shear flow. *Bull. Am. Phys. Soc.* **22**, 1285.
- BROWN, G. L. & ROSHKO, A. 1974 On density effects and large structures in turbulent mixing layers. *J. Fluid Mech.* **64**, 775–816.
- BRUMLEY, B. & JIRKA, H. 1987 Near-surface turbulence in a grid stirred tank. *J. Fluid Mech.* **183**, 235–263.
- DABIRI, D. & GHARIB, M. 2001 Simultaneous free surface deformation and near surface velocity measurements. *Exps. Fluids* **30**, 381–390.
- DABIRI, D., ZHANG, X. & GHARIB, M. 1994 A real-time free surface elevation mapping technique. *Seventh Intl Symp. on Applications of Laser Techniques to Fluid Mechanics, Lisbon, Portugal, July 11–14* (ed. R. J. Adrian, D. F. G. Durão, F. Durst, M. V. Heitor, M. Maeda & J. H. Whitelaw).
- DABIRI, D., ZHANG, X. & GHARIB, M. 1997 Quantitative visualization of three-dimensional free surface slopes and elevations. In *Atlas of Visualization* (ed. Y. Nakayama). CRC Press.
- DOMMERMUTH, D. G. 1994 The initialization of vortical free surface flows. *Trans. ASME: J. Fluids Engng* **116**, 95–102.

- DOMMERMUTH, D. G., NOVIKOV, E. & MUI, R. 1994 The interaction of surface waves with turbulence. *free-surface Turbulence ASME Meeting*. FED-Vol. 181 (ed. E. P. Rood & J. Katz), pp. 123–140.
- GEORGE, W. K., BEUTHER, P. D. & ARNDT, R. E. A. 1984 Pressure spectra in turbulent free shear flows. *J. Fluid Mech.* **148**, 155–191.
- GHARIB, M. & WEIGAND, A. 1996 Experimental studies of vortex disconnection and connection at a free surface. *J. Fluid Mech.* **321**, 59–86.
- GHARIB, M., WEIGAND, A., WILLERT, C. & LIEPMANN, D. 1992 Experimental studies of vortex reconnection to a free surface: a physical flow model. *Proc. 19th Symp. on Nav. Hydrodyn.*, pp. 507–525. Washington DC: Natl Acad.
- GREGA, L. M., WEI, T., LEIGHTON, R. I. & NEVES, J. C. 1995 Turbulent mixed-boundary flow in a corner formed by a solid wall and a free surface. *J. Fluid Mech.* **294**, 17–46.
- HUNT, J. C. R. & GRAHAM, J. M. R. 1978 Free-stream turbulence near plane boundaries. *J. Fluid Mech.* **84**, 209–235.
- JÄHNE, B. 1997 *Image Processing for Scientific Applications*. CRC Press.
- JÄHNE, B. & HAUBECKER, H. 1998 Air–water gas exchange. *Annu. Rev. Fluid Mech.* **30**, 443–468.
- LOGORY, L. M., HIRSA, A. & ANTHONY, D. G. 1996 Interaction of wake turbulence with a free surface. *Phys. Fluids* **8**, 805–815.
- LONGO, J., HUANG, H. P. & STERN, F. 1998 Solid/Free-surface juncture boundary layer and wake. *Exps. Fluids* **25**, 283–297.
- LUGT, H. J. & OHRING, S. 1992 The oblique ascent of a viscous vortex pair toward a free surface. *J. Fluid Mech.* **236**, 461–476.
- MAHEO, P. M. 1999 Free surface turbulent shear flows. PhD thesis. California Institute of Technology.
- MELVILLE, W. K. 1996 The role of surface-wave breaking in air–sea interaction. *Annu. Rev. Fluid Mech.* **28**, 279–321.
- MONIN, A. & YAGLOM, A. M. 1975 *Statistical Fluid Mechanics*, Vol. II. MIT Press.
- PEREIRA, F., GHARIB, M., DABIRI, D. & MODARRESS, D. 2000 Defocusing DPIV: A 3-component 3-D DPIV measurement technique. Application to bubbly flows. *Exps. Fluids* **29**, S078–S084.
- ROOD, E. P. 1994 Interpreting vortex interaction with a free surface. *Trans. ASME: J. Fluids Engng* **116**, 91–94.
- SARPKAYA, T. & NEUBERT, D. E. 1994 Interaction of a streamwise vortex with a free surface *AIAA J.* **32**, 594–600.
- SARPKAYA, T. & SUTHON, P. 1991 Interaction of a vortex couple with a free surface. *Exps. Fluids* **11**, 205–217.
- SHEN, L., TRIANTAFYLLOU, G. S. & YUE, D. K. P. 2000 Turbulent diffusion near a free surface. *J. Fluid Mech.* **407**, 145–166.
- SHEN, L., ZHANG, X., YUE, D. K. P. & TRIANTAFYLLOU, G. S. 1999 The surface layer for free surface turbulent flows. *J. Fluid Mech.* **386**, 167–212.
- SWEAN, T. F., RAMBERG, S. E. & MINER, E. W. 1991 Anisotropy in a turbulent jet near a free surface. *Trans. ASME: J. Fluids Engng* **113**, 430–438.
- TSAI, W. T. 1998 A numerical study of the evolution of structure of turbulent shear layer under a free surface. *J. Fluid Mech.* **354**, 239–276.
- WALKER, D. T. & JOHNSTON, V. G. 1991 Observations of turbulence near the free surface in the wake of a model ship. In *Dynamics of Bubbles and Vortices Near a Free Surface* (ed. I. Sahin & G. Tryggvason). ASME AMD-119.
- WALKER, D. T., LEIGHTON, R. I. & GARZA-RIOS, L. O. 1996 Shear-free turbulence near a flat free surface. *J. Fluid Mech.* **320**, 19–51.
- WEIGAND, A. & GHARIB, M. 1995 Turbulent vortex ring/free surface interaction. *Trans. ASME: J. Fluids Engng.* **117**, 374–381.
- WILLERT, C. E. & GHARIB, M. 1997 The interaction of spatially modulated vortex pairs with free surfaces. *J. Fluid Mech.* **345**, 227–250.
- WOOLF, D. K. & THORPE, S. A. 1991 Bubbles and the air–sea exchange of gases in near-saturation conditions. *J. Mar. Res.* **49**, 435–466.
- ZHANG, X. & COX, C. S. 1994 Measuring the two-dimensional structure of a wavy water surface optically: a surface gradient detector. *Exps. Fluids* **17**, 225–237.
- ZHANG, C., SHEN, L., & YUE, D. K. P. 1999 The mechanism of vortex connection at a free surface. *J. Fluid Mech.* **384**, 207–241.